Published in final edited form as:
Nat Cell Biol. 2016 January ; 18(1): 122–131. doi:10.1038/ncb3273.

TMEM107 recruits ciliopathy proteins to subdomains of the ciliary transition zone and causes Joubert syndrome

Nils J. Lambacher[#1], **Ange-Line Bruel**[#2], **Teunis J. P. van Dam**[#3], **Katarzyna Szymańska**[4], **Gisela G. Slaats**[5], **Stefanie Kuhns**[1], **Gavin J. McManus**[6], **Julie E. Kennedy**[1], **Karl Gaff**[1], **Ka Man Wu**[5], **Robin van der Lee**[3], **Lydie Burglen**[7], **Diane Doummar**[7], **Jean-Baptiste Rivière**[2,8], **Laurence Faivre**[2,8], **Tania Attié-Bitach**[9,10,11], **Sophie Saunier**[9,10], **Alistair Curd**[12], **Michelle Peckham**[12], **Rachel H. Giles**[5], **Colin A. Johnson**[4], **Martijn A. Huynen**[3,*], **Christel Thauvin-Robinet**[2,8,*], and **Oliver E. Blacque**[1,*]

[1]School of Biomolecular and Biomedical Science, UCD Conway Institute, University College Dublin, Belfield, Dublin 4, Ireland [2]EA4271 GAD, Genetics of Development Abnormalities, Burgundy University, Dijon, France [3]Centre for Molecular and Biomolecular Informatics, Radboud Institute for Molecular Life Sciences, Radboud university medical center, Geert Grooteplein 26-28, 6525 GA Nijmegen, Netherlands [4]Section of Ophthalmology and Neurosciences, Leeds Institute of Biomolecular & Clinical Sciences, University of Leeds, Leeds, LS9 7TF, UK [5]Department of Nephrology and Hypertension, University Medical Center Utrecht, Utrecht, The Netherlands [6]School of Biochemistry and Immunology, Microscopy facility, Trinity Biomedical Sciences Institute, Trinity College Dublin, 152-160 Pearse Street, Dublin 2, Ireland [7]Service de Neuropédiatrie, laboratoire de Neurogénétique Moléculaire, Hôpital d'Enfants Armand-Trousseau, CHU Paris Est, France [8]8FHU TRANSLAD, CHU Dijon, France [9]INSERM UMR1163, Hôpital Necker-Enfants Malades, Paris, France [10]Université Paris Descartes, Sorbonne Paris Cité, France, Institut IMAGINE, Paris, France [11]Département de Génétique, Hôpital Necker-Enfants Malades, AP-HP, Paris, France [12]School of Molecular and Cellular Biology, Faculty of Biological Sciences, University of Leeds, Leeds, UK

[#] These authors contributed equally to this work.

Abstract

Correspondence to: oliver.blacque@ucd.ie, martijn.huijnen@radboudumc.nl, christel.thauvin@chu-dijon.fr.
[*]Co-corresponding authors

Author Contributions

N.J.L., J.E.K., K.G and O.E.B. performed and interpreted experiments with *C. elegans*. T.J.P.v.D., R.v.d.L. and M.A.H. performed all bioinformatics analyses. A-L.B., L.B., D.D., T.A-B., S.S., and C.T-R collected, purified patient samples, performed exome sequencing and analysed sequencing data. N.J.L., S.K., G.J.M. performed the STED imaging. A.C., M.P and C.A.J conducted the dSTORM imaging and processing. K.S., S.K, G.G.S., K.M.W., and R.H.G. conducted transfection and immunofluorescence microscopy in mammalian cells. K.S. and C.A.J. contributed the co-immunoprecipitation experiments. J-B.R., L.F. and C.T-R. diagnosed and referred patients. The co-corresponding authors shared supervision of the work. M.A.H. uncovered TMEM107 as a candidate ciliary gene, and directed the bioinformatics work. C.T-R. collated JBTS and OFD patient samples, performed clinical characterisation and directed the sequencing. O.E.B. directed research, analysed and collated data for the manuscript. O.E.B., M.A.H, R.H.G., and C.A.J. conceived and executed the study, and O.E.B., N.J.L., T.J.v.D., and M.A.H. wrote the manuscript.

Competing Financial Interest Statement

The authors declare no competing financial interest in relation to this work.

Europe PMC Funders Author Manuscripts

The transition zone (TZ) ciliary subcompartment is thought to control cilium composition and signaling by facilitating a protein diffusion barrier at the ciliary base, and TZ defects cause ciliopathies such as Meckel-Gruber syndrome (MKS), nephronophthisis (NPHP) and Joubert syndrome (JBTS) 1. However, the molecular composition and mechanisms underpinning TZ organisation and barrier regulation are poorly understood. To uncover candidate TZ genes, we employed bioinformatics (co-expression and co-evolution) and identified TMEM107 as a TZ protein mutated in oral-facial-digital syndrome (OFD) and JBTS patients. Mechanistic studies in *Caenorhabditis elegans* showed TMEM107 controls ciliary composition and functions redundantly with NPHP4 to regulate cilium integrity, TZ docking and assembly of membrane to microtubule Y-link connectors. Furthermore, nematode TMEM107 occupies an intermediate layer of the TZ-localised MKS module by organising recruitment of ciliopathy proteins MKS1, TMEM231 (JBTS20) and TMEM237 (JBTS14). Finally, MKS module membrane proteins are immobile and super-resolution microscopy (STED, dSTORM) in worms and mammalian cells reveals periodic localisations within the TZ. This work expands the MKS module of ciliopathy-causing TZ proteins associated with diffusion barrier formation and provides insight into TZ subdomain architecture.

Cilia are microtubule-based structures serving motility, sensory, and signaling functions, and ciliary defects cause broad spectrum symptoms including cystic kidneys, blindness and nervous system defects2. Cilia possess subcompartments with distinct molecular compositions, enriched for receptors, channels, and signaling components3. Protein targeting to cilia depends on intraflagellar transport (IFT) and membrane trafficking pathways that sort, deliver and recycle ciliary components4. A recently established paradigm implicates ‘gated’ diffusion barriers at the ciliary base that regulate protein entry in a size-dependent manner and restrict lateral transport between ciliary and non-ciliary membranes1, 5–10.

The ciliary gate is associated with the proximal-most 0.2-0.8 μm of the axoneme, termed TZ, characterised by Y-shaped structures that connect the microtubules and membrane. Y-links are also thought to organise the ciliary necklace, a membrane specialisation consisting of intramembranous particles that may contribute to diffusion barrier properties11, 12. Multiple MKS, JBTS and NPHP proteins are TZ-localised and regulate ciliary composition and signaling 5–7, 13. In *C. elegans* (Ce) sensory neurons, 13 ciliopathy protein orthologues localise at the TZ, where they functionally associate as MKS (MKS-1, MKS-2, MKS-3, MKS-5, MKS-6, MKSR-1, MKSR-2, JBTS-14, TMEM-17, TMEM-231), NPHP (NPHP-1, NPHP-4) or CEP-290-associated modules to regulate Y-link formation and TZ docking during cilium assembly10, 13–19.

To predict new TZ genes, we employed a weighted gene co-expression screening strategy 20, and a training set of 20 known TZ genes (Supplementary Table 1)1, to interrogate >1600 mouse and human expression microarray datasets in GEO (Supplementary Table 2; top 500 co-expressed genes shown in Supplementary Table 3). In the integrated datasets, TZ genes display higher co-expression with each other than genomic background (Mann-Whitney *U* tests: $p=1.57e^{-14}$ (human); $p=1.42e^{-9}$ (mouse); Fig. 1a and Supplementary Fig. 1a). Ciliary genes21 are also enriched (Mann-Whitney *U* tests: $p=7.35e^{-55}$ (human); $p=1.43e^{-44}$

(mouse)), but less than TZ genes (Mann-Whitney *U* tests: $p=1.36e^{-10}$ (human); $p=1.01e^{-6}$ (mouse); (Fig. 1a and Supplementary Fig. 1a). Cross validation (leave-one-out analysis) shows that our method retrieves TZ genes versus ciliary genes, although this is not pronounced among top scoring genes (Fig. 1b).

We compared the top 100 co-expressed human and mouse genes and identified 18 common genes, of which 13 encode proteins with known cilia associations (Supplementary Table 3). For the remaining 5 genes, we examined the genomes of ciliated species lacking a TZ (*Physcomitrella patens*, *Selaginella moellendorffii, Plasmodium falciparum* and *Giardia intestinalis*22) and found a TZ phylogenetic distribution for *TMEM107* (Supplementary Fig. 1b). Although this gene was previously shown to regulate mammalian ciliogenesis and Shh signaling23, the basis of these functions is unknown.

In *C. elegans*, the TMEM107 orthologue (F39B2.9; TMEM-107) is exclusively expressed in ciliated cells and localises at the TZ (Fig. 1c and Supplementary Fig. 2a). Like other TZ genes, worm and human *TMEM107* possess X-box promoter motifs and nematode *tmem-107* expression is exclusively dependent on the RFX transcription factor DAF-19 (Supplementary Fig. 2b, c). TMEM107 possesses four predicted transmembrane helices and short cytosolic N- and C-termini (Supplementary Fig. 1c, d). Disruption of the nematode transmembrane domain linkers or cytosolic N- or C- termini did not affect localisation, suggesting that TMEM-107's TZ association depends on its transmembrane helices (Supplementary Fig. 2d). Similar to *C. elegans* TMEM-107, human TMEM107::GFP also localises at the TZ (Fig. 1d).

The TZ localisation, combined with reported ciliogenesis and signaling roles23, makes *TMEM107* a strong ciliopathy gene candidate. Indeed, similar to observations for other ciliopathy gene disruptions24 and the *Tmem107 Schlei* mouse23, *Tmem107*-depleted IMCD3 cells display reduced ciliation and lumen size in 3D spheroids (Fig. 2a, b). To explore disease associations, *TMEM107* exons were screened for mutations in 238 JBTS or OFD type VI individuals using Sanger and next generation sequencing. We identified a homozygous missense variant (NM_183065: g.8079298T>C; p.Glu45Gly) in OFDVI female twins with consanguineous parents, and a compound heterozygous mutation comprising a frameshift deletion (NM_032354.3: g.8077560delT; p.Leu134Phe*fs**8) and an in-frame codon deletion (NM_032354.3: g.8077890_8077893delGAA; p.Phe106del) in a JBTS male (Fig. 2c and Supplementary Fig. 3a,b). All patients possess similar neurological disturbances, retinopathy, and the JBTS-associated molar tooth sign (Fig. 2d-g and Supplementary Fig. 3c). The females were diagnosed with OFDVI because they also displayed hamartoma and frenulae phenotypes (Supplementary Fig. 3c). All three variants segregated in the families, were predicted to be pathogenic by Human Splicing Finder and PolyPhen2, and were absent in the heterozygous and homozygous state in human variation databases (NHLBI Exome Variant Server, ExAC). In further support of pathogenicity, fibroblasts from the JBTS male displayed reduced ciliation, and those cilia that formed were abnormally long (Fig. 2h-j). The latter contrasts with the short cilia of hypomorphic *Schlei* mouse fibroblasts, carrying a missense mutation (E125G) in Tmem10723; which may be explained by cell type, species or allelic distinctions. We could not use complementation experiments to investigate how the patient mutations affect TMEM107 function because

even moderate TMEM107(WT) over-expression was toxic to fibroblast cilium formation. However, TMEM107(E45G) and TMEM107(F106del) retained the ability to localise at the TZ, indicating that these mutations exert their pathogenicity by disrupting TMEM107 functions at the TZ, rather than a gross effect on TMEM107 localisations or stability (Supplementary Fig. 2e).

Next, we investigated the role of TMEM107 in *C. elegans* TZs. Since loss-of-function alleles were unavailable, we used CRISPR-Cas925 to isolate *oq100*, a 27-bp deletion + 14-bp insertion (Fig. 3a). This mutation causes a frame-shift and premature stop, which disrupts transmembrane domains 3 & 4, and is likely a null allele as *tmem-107(oq100)::GFP* is not expressed (Fig. 3b). *tmem-107(oq100)* mutants appear normal for dye-filling (indirect measure of cilium integrity26), cilium length and morphology, and amphid cilium ultrastructure (Fig. 3c, d and Supplementary Fig. 4a). Also, *tmem-107* mutants possess normal cilia-related chemoattraction and foraging sensory behaviours (Fig. 3e). Thus, *tmem-107* loss does not grossly affect cilium structure and function.

We examined if *tmem-107* functions redundantly with other TZ genes and found a synthetic genetic interaction with *nphp-4*. Like worms with mutations in a *C. elegans* MKS *and* an NPHP module gene10, 15, *tmem-107;nphp-4* double mutants display defects in dye-filling, cilium length and morphology and sensation (Fig. 3c-e). The synthetic cilium structure defects were confirmed by TEM, which showed that 3-5 amphid pore cilia are truncated or missing in *nphp-4;tmem-107* mutants, whereas most or all axonemes are present in the corresponding single mutants (Supplementary Fig. 4a). Conversely, *tmem-107* does not synthetically interact with *mksr-1* as assessed by dye filling (Fig. 3c), suggesting that *tmem-107* is part of the MKS module whose genes synthetically interact with NPHP module genes but not with each other10, 15, 27. Importantly, transgenic expression of *tmem-107(WT)::gfp* in *tmem-107;nphp-4* worms rescued the cilium structure and function phenotypes, confirming phenotypic linkage to *oq100* (Fig. 3c, e). Surprisingly, *tmem-107* constructs mimicking the human TMEM107 patient mutations also rescued the *tmem-107;nphp-4* Dyf phenotype (Supplementary Fig. 4c), and in agreement with these variants retaining functionality, the encoded proteins localised normally (Supplementary Fig. 2b).

TZ ultrastructure was also disrupted in *tmem-107;nphp-4* worms compared to single mutants of *tmem-107* (unaffected) and *nphp-4* (modestly affected; discussed below). In double mutants, Y-links were reduced or missing, and in agreement with loss of these membrane-microtubule connectors, many TZs were undocked from the plasma membrane, frequently extending from ectopic positions within the distal dendrite (Supplementary Fig. 4b). Also, *tmem-107;nphp-4* mutant cilia often displayed abnormal vesicle accumulations in the TZ and PCMC regions (Supplementary Fig. 4b). Consistent with these structural defects, MKS-2 TZ localisation is disrupted in *tmem-107;nphp-4* worms, but not in single mutants (Fig. 3f; *nphp-4* data shown in ref 15). Furthermore, *tmem-107;nphp-4* neuronal dendrites (phasmids) are frequently short, indicating dendritic tip anchoring defects during dendrite elongation (Fig. 3g)10, 17, 27. Thus, like known MKS module components, TMEM-107 functionally interacts with NPHP-4 to facilitate TZ formation, composition and dendrite formation.

As mentioned above, *nphp-4* single mutants display modest ultrastructural TZ defects, despite previous reports that TZs were normal in these worms16. In *nphp-4* worms carrying *tm925* (deletion) or *gk529336* (nonsense) mutations, Y-link densities were frequently reduced and sometimes missing, and undocked TZs were observed in ADF and ADL neurons (Supplementary Fig. 4b). Thus, *C. elegans nphp-4* alone regulates aspects of Y-link assembly or stability, which agrees with the mild cilium structure defects in corresponding mutants (Supplementary Fig. 4a; also ref 16). We conclude that NPHP and MKS modules are not fully redundant in building TZs in at least some amphid channel neurons.

Similar to known MKS module gene mutants10, 15, 19, TRAM-1 abnormally leaks into *tmem-107* mutant cilia, demonstrating membrane diffusion barrier defects and altered ciliary composition in these worms (Fig. 3h). However, membrane-associated RPI-2 does not leak into *tmem-107(oq100)* cilia indicating the barrier is selectively disrupted (Fig. 3h), which contrasts with other MKS module gene mutants, where both TRAM-1 and RPI-2 leak into cilia10.

To further investigate TMEM107 associations with MKS module proteins, and the evolutionary conservation of these interactions, three complementary approaches were taken. First, we employed protein localisation dependency assays. In *C. elegans*, the MKS module is proposed to assemble hierarchically10, 13, 15, 19. In this model, MKS-5 occupies the root of the hierarchy (Layer 1), required for TZ localisation of all MKS module components. In contrast, MKS-3, JBTS-14, MKS-6 and TMEM-17 occupy a peripheral level (Layer 3) not required for localisation of other proteins, whereas MKSR-1, MKSR-2, TMEM-231 and MKS-2 form an intermediate level (Layer 2), required for Layer 3 but not Layer 1 protein targeting. To evaluate if TMEM-107 is part of this model, TMEM-107::GFP localisation was assessed in MKS module gene mutants, and MKS module protein localisations were analysed in *tmem-107(oq100)* mutants. We found TMEM-107 is not required for Layer 1 and most Layer 2 protein localisations, but is required for the organisation of Layer 3 proteins (JBTS-14, TMEM-17), as well as MKS-1 (unassigned layer) and TMEM-231 (layer 2) (Fig. 4a). In reverse experiments, TMEM-107 localisation depends on Layer 1, 2 and MKS-1 proteins, but not Layer 3 proteins (Fig. 4a). Furthermore, TMEM-107 and NPHP module proteins are not localisation interdependent (Fig. 4a). These data show that TMEM-107 recruits an MKS submodule of proteins (TMEM-17, TMEM-231, JBTS-14, MKS-1) and suggest that TMEM-107 occupies an intermediate layer, connecting Layer 2 to a Layer 3 subset (Fig. 4b). Interestingly, TZ recruitment of TMEM-17 and TMEM-231 by TMEM-107 is independent of its short cytosolic N- and C- termini, suggesting this function is orchestrated by the transmembrane helices or interhelical linkers (Fig. 4c). In agreement with our nematode data, depletion of mammalian *Tmem107* also alters the localisation of some MKS module proteins (Tmem231 and Tmem237) but not others (Rpgrip1l) (Fig. 4d).

In the second approach, co-immunoprecipitation (coIP) assays were performed to determine if mammalian TMEM107 biochemically associates with MKS module proteins. GFP-tagged TMEM107 was exogenously co-expressed with FLAG-tagged TMEM216, TMEM231, TMEM17 or TMEM237, or with myc-tagged MKS1, and assessed for associations in IMCD3 cells using binding conditions optimized for membrane proteins28. We found

TMEM107 immunoprecipitates full-length TMEM216, TEMM231, TMEM 237 and MKS1, but not TMEM17 (Fig. 4e). For TMEM237, TMEM107 did not detectably interact with an N-terminal cytoplasmic domain of this protein (TMEM237Nt), indicating the TMEM237 association depends on its transmembrane helices or C-terminal cytoplasmic domain (Fig. 4e).

In the third approach, we used differential Dollo parsimony29 to obtain co-evolutionary relationships for MKS module proteins. In agreement with the nematode hierarchy10, 15, Layer 2 orthologues TMEM216, B9D1 and B9D2 form a co-evolving MKS core (Fig. 4f). This ‘core’ co-evolves with Layer 3 orthologues TMEM67 and CC2D2A, consistent with localisation dependencies in mammalian systems5, though not in worms (Fig. 4f). We also identified a co-evolving TMEM107, TMEM17 and TMEM231 submodule, again agreeing with nematode localisation dependencies (Fig. 4f). Unexpectedly, this submodule does include TMEM237 because orthologues are missing in stramenopiles, alveolates and excavates (Supplementary Fig. 1b), indicating late incorporation into the MKS module. Also surprising was that RPGRIP1L only marginally co-evolves with the MKS module, despite its central role in module organisation10, 19 (Fig. 4f). This may be explained by low RPGRIP1L sequence conservation and difficulties in assigning orthologues. Finally, the interdependent MKS1 and TMEM107 localisations are not reflected in the co-evolution data. Thus, our evolutionary findings support conserved roles for *C. elegans* TMEM107 in organising an MKS submodule with TMEM231 and TMEM17, but differences in the modular arrangements of TMEM107 with other MKS proteins might exist between species.

The specific TZ localisation of MKS module proteins, together with their requirement for Y-link assembly with NPHP proteins, could suggest this module interacts with Y-links or associated structures. If true, MKS module proteins should be immobile. Using fluorescence recovery after photobleaching (FRAP) assays in *C. elegans*, photobleaching one half of the TZ signal for TMEM-107::GFP, MKS-2::GFP and MKS-6::GFP resulted in no signal recovery (30 minutes), indicating that the non-bleached TZ pool is immobile (Fig. 5a). Also, no recovery was observed when entire TZ signals were photobleached (MKS-2::GFP), demonstrating that MKS module proteins possess slow TZ entry kinetics (Supplementary Fig. 5a). This immobility depends on other MKS module proteins because MKS-2 is highly mobile in *mksr-1* (B9D1) mutants (Fig. 5b). Therefore, we conclude that transmembrane (TMEM-107, MKS-2) and membrane-associated (MKS-6) proteins are anchored at the TZ membrane. Furthermore, at least for MKS-2, anchoring requires an intact MKS module.

Next, we used stimulated emission depletion (STED) super-resolution microscopy to further investigate *C. elegans* MKS (TMEM-107, MKS-2 and TMEM-231) and NPHP (NPHP-1) module protein distributions within TZs. Side view TZ images (axial orientation) revealed that these proteins are periodically distributed along the axial plane, frequently appearing as multiple independent rings (partial or complete), or possibly spiral structures (Fig. 5c and Supplementary Fig. 5b). However, in some images with slightly better resolution, individual dots of signal were evident within ring-like domains (Fig. 5c; arrowheads), suggesting these domains consist of multiple discrete protein clusters. Punctate signals were also observed for NPHP-1, suggesting MKS and NPHP module proteins possess similar axial TZ distributions

(Fig. 5c). We were unable to determine protein distributions from true traverse (radial) views of the TZ because of the orientation of worms (and cilia) on the imaging slide.

We also performed STED imaging on endogenous RPGRIP1L and TMEM67 in human cells (RPTEC-TERT1). Imaging of TZs in radial orientation revealed that these proteins can form discrete clusters arranged as a complete or near complete single shallow ring (Fig. 5d and Supplementary Fig. 5c). Although the number of resolved clusters was variable, rings with 7-8, or possibly 9 clusters were observed. In addition, RPGRIP1L ring diameters were significantly narrower than TMEM67 ring diameters (Fig. 5d). As an alternative approach, we imaged endogenous RPGRIP1L using direct stochastic optical reconstruction microscopy (dSTORM). Similar to our STED findings, dSTORM imaging of RPGRIP1L revealed a single shallow ring of TZ signal, comprised of at least 7-8 independent punctae (Fig. 5e and Supplementary Fig. 5d). Thus, both mammalian RPGRIP1L and TMEM67 appear to be organised as discrete clusters within ring-like domains of differing diameters, indicating distinct radial positioning at the TZ membrane (TMEM67) and core (RPGRIP1L). The periodicity of the clusters approaches the 9 fold symmetry of Y-links, suggesting possible association with these structures.

Together, our super-resolution imaging indicates that MKS module proteins occupy periodic radial and axial subdomains of the TZ core and membrane (Fig. 5f). The nematode axial pattern is reminiscent of the ciliary necklace, a conserved TZ membrane specialisation comprised of 1-7 rows of intramembrane leaflet particles identified almost 40 years ago11, 12 (Fig. 5f). In further support of a necklace association, *C. elegans* MKS module proteins are anchored at the TZ membrane, and the periodic radial distribution of mammalian TMEM67 at the TZ membrane approaches the periodicity of Y-links implicated in necklace formation11. In one model, Y-links would anchor MKS module proteins at the necklace (Fig. 5f). However, a tomographic (TEM) reconstruction of a portion of the *C. elegans* TZ indicates that Y-links are continuous structures running the TZ length (Supplementary Video 1 and Fig. 5f; also ref 18); thus, any association of MKS proteins with Y-links would occur at various axial positions along continuous Y-link sheets (Fig. 5f). Unfortunately, we could not identify a necklace pattern for mammalian MKS module proteins because of spatial constraints and resolution limits conferred by the short TZ (<200 nm). Future super-resolution imaging on mammalian cells with longer TZs should clarify the nematode observations.

In summary, we have identified TMEM107 as a ciliopathy TZ protein and conserved MKS module component. Causality of the mutations identified here to JBTS and OFDVI is supported by very recent reports of additional *TMEM107* mutations linked to MKS and OFD 30, 31. Furthermore, we show that ciliopathy proteins are anchored at the TZ membrane, and display periodic radial and axial distributions at the TZ core and membrane. In addition, our finding that MKS-2 is mobile in *mksr-1* (B9D1) mutant cilia indicates that protein anchoring at the TZ is important for barrier functions. Strikingly, membrane diffusion barriers of the axon initial segment (AIS) that limit free exchange of phospholipids also depend on anchored membrane proteins32, and sodium channels within the AIS membrane are coordinately localised with evenly spaced (180-190 nm) actin-spectrin cytoskeletal rings33. Thus, the TZ and AIS cellular compartments may share comparable

molecular organisation underpinning common mechanisms of barrier function. Finally, our bioinformatics analysis to discover genes of the TZ compartment goes beyond most comparative genomics studies that focus on the entire cilium. Indeed, distinct phylogenetic distributions exist for other ciliary modules such as IFT-A, IFT-B and BBSome assemblies34. Thus, exploitation of genomics data can help to disentangle ciliary modules, ultimately leading to greater understanding of ciliary transport, signaling and disease.

Supplementary Material

Refer to Web version on PubMed Central for supplementary material.

Acknowledgements

This work was funded via the European Community's Seventh Framework Programme FP7/2009 (SYSCILIA grant agreement 241955; to OEB, MAH, RHG, CAJ, and Gencodys; to MAH), Science Foundation Ireland (11/PI/1037 to OEB), the Dutch Kidney Foundation CP11.18 “KOUNCIL” (to RHG), the GIS-Institut des Maladies Rares (HTS; to C. T-R), the French Fondation for Rare Disease (to CTR), the Virgo consortium (FES0908; to MAH), the Netherlands Genomics Initiative (050-060-452; RvdL; to MAH), the French Ministry of Health (PHRC national 2010-A01014-35 and 2013; to CTR), the Fondation pour la Recherche Médicale (DEQ20130326532; to SS), the Regional Council of Burgundy (to CTR), a Sir Jules Thorn Award for Biomedical Research (JTA/09; to CAJ), and the UK Medical Research Council (MR/K011154/1 to CAJ, and MR/K015613/1; to MP). We thank the patients and their families for their participation. We also thank the NHLBI GO Exome Sequencing Project and its ongoing studies which produced and provided exome variant calls for comparison: the Lung GO Sequencing Project (HL-102923), the WHI Sequencing Project (HL-102924), the Broad GO Sequencing Project (HL-102925), the Seattle GO Sequencing Project (HL-102926) and the Heart GO Sequencing Project (HL-103010). We thank Michel Leroux (Simon Fraser University, Canada), Brad Yoder (University of Alabama, USA), the *Caenorhabditis elegans* genetic center (Minnesota, USA), the National Bioresource project (Tokyo, Japan), the International *C. elegans* gene knockout consortium, and the *C. elegans* Million Mutation Project for nematode reagents. We are grateful to Christian Eggeling and Christopher Lagerholm (Weatherall Institute of Molecular Medicine and the Wolfson Imaging Center, Oxford, UK) for assistance with STED microscopy, Dimitri Scholz and Tiina Toivonen (UCD Conway Institute imaging facility, Dublin, IRL) for imaging support, and Remko Dijkstra (Scientific Volume Imaging bv, Hilversum, NL) for assistance with STED image deconvolution. We also thank Alexa Cleasby (Faculty of Biological Sciences, University of Leeds, Leeds, UK) for help with developing the dSTORM technique, Dr. Ben Chih (Genentech Inc., South San Francisco, CA, USA) for the kind gift of polyclonal anti-TMEM17 and TMEM231 antibodies, and Dr. Tara McMorrow (University College Dublin, Dublin, Ireland) for the generous gift of the RPTEC/TERT1 cells. We thank Diana Rodriguez (Trousseau hospital, Paris) for assistance with analysis of brain MRIs. The dSTORM microscope was generously funded by alumnus Michael Beverly, in support of the University of Leed’s ‘making a world of difference campaign’.

References

1. Reiter J, Blacque O, Leroux M. The base of the cilium: roles for transition fibres and the transition zone in ciliary formation, maintenance and compartmentalization. EMBO reports. 2012; 13:608–618. [PubMed: 22653444]
2. Goetz SC, Anderson KV. The primary cilium: a signalling centre during vertebrate development. Nat Rev Genet. 2010; 11:331–344. [PubMed: 20395968]
3. Blacque OE, Sanders AA. Compartments within a compartment: what C. elegans can tell us about ciliary subdomain composition, biogenesis, function, and disease. Organogenesis. 2014; 10:126–137. [PubMed: 24732235]
4. Hsiao YC, Tuz K, Ferland RJ. Trafficking in and to the primary cilium. Cilia. 2012; 1:4. [PubMed: 23351793]
5. Chih B, et al. A ciliopathy complex at the transition zone protects the cilia as a privileged membrane domain. Nature cell biology. 2011; 14:61–72. [PubMed: 22179047]
6. Craige B, et al. CEP290 tethers flagellar transition zone microtubules to the membrane and regulates flagellar protein content. The Journal of cell biology. 2010; 190:927–940. [PubMed: 20819941]
7. Garcia-Gonzalo FR, et al. A transition zone complex regulates mammalian ciliogenesis and ciliary membrane composition. Nature genetics. 2011; 43:776–784. [PubMed: 21725307]

8. Hu Q, et al. A septin diffusion barrier at the base of the primary cilium maintains ciliary membrane protein distribution. Science (New York N.Y. 2010; 329:436–439.
9. Kee HL, et al. A size-exclusion permeability barrier and nucleoporins characterize a ciliary pore complex that regulates transport into cilia. Nature cell biology. 2012; 14:431–437. [PubMed: 22388888]
10. Williams CL, et al. MKS and NPHP modules cooperate to establish basal body/transition zone membrane associations and ciliary gate function during ciliogenesis. The Journal of cell biology. 2011; 192:1023–1041. [PubMed: 21422230]
11. Gilula NB, Satir P. The ciliary necklace. A ciliary membrane specialization. The Journal of cell biology. 1972; 53:494–509. [PubMed: 4554367]
12. Heller RF, Gordon RE. Chronic effects of nitrogen dioxide on cilia in hamster bronchioles. Experimental lung research. 1986; 10:137–152. [PubMed: 3956447]
13. Roberson EC, et al. TMEM231, mutated in orofaciodigital and Meckel syndromes, organizes the ciliary transition zone. The Journal of cell biology. 2015; 209:129–142. [PubMed: 25869670]
14. Cevik S, et al. Active Transport and Diffusion Barriers Restrict Joubert Syndrome-Associated ARL13B/ARL-13 to an Inv-like Ciliary Membrane Subdomain. PLoS genetics. 2013; 9:e1003977. [PubMed: 24339792]
15. Huang L, et al. TMEM237 Is Mutated in Individuals with a Joubert Syndrome Related Disorder and Expands the Role of the TMEM Family at the Ciliary Transition Zone. American journal of human genetics. 2011; 89:713–730. [PubMed: 22152675]
16. Jauregui AR, Nguyen KC, Hall DH, Barr MM. The Caenorhabditis elegans nephrocystins act as global modifiers of cilium structure. The Journal of cell biology. 2008; 180:973–988. [PubMed: 18316409]
17. Williams CL, Winkelbauer ME, Schafer JC, Michaud EJ, Yoder BK. Functional redundancy of the B9 proteins and nephrocystins in Caenorhabditis elegans ciliogenesis. Mol Biol Cell. 2008; 19:2154–2168. [PubMed: 18337471]
18. Schouteden C, Serwas D, Palfy M, Dammermann A. The ciliary transition zone functions in cell adhesion but is dispensable for axoneme assembly in C. elegans. The Journal of cell biology. 2015; 210:35–44. [PubMed: 26124290]
19. Jensen VL, et al. Formation of the transition zone by Mks5/Rpgrip1L establishes a ciliary zone of exclusion (CIZE) that compartmentalises ciliary signalling proteins and controls PIP2 ciliary abundance. The EMBO journal. 2015
20. Baughman JM, et al. A computational screen for regulators of oxidative phosphorylation implicates SLIRP in mitochondrial RNA homeostasis. PLoS genetics. 2009; 5:e1000590. [PubMed: 19680543]
21. van Dam TJ, Wheway G, Slaats GG, Huynen MA, Giles RH. The SYSCILIA gold standard (SCGSv1) of known ciliary components and its applications within a systems biology consortium. Cilia. 2013; 2:7. [PubMed: 23725226]
22. Barker AR, Renzaglia KS, Fry K, Dawe HR. Bioinformatic analysis of ciliary transition zone proteins reveals insights into the evolution of ciliopathy networks. BMC genomics. 2014; 15:531. [PubMed: 24969356]
23. Christopher KJ, Wang B, Kong Y, Weatherbee SD. Forward genetics uncovers Transmembrane protein 107 as a novel factor required for ciliogenesis and Sonic hedgehog signaling. Dev Biol. 2012; 368:382–392. [PubMed: 22698544]
24. Giles RH, Ajzenberg H, Jackson PK. 3D spheroid model of mIMCD3 cells for studying ciliopathies and renal epithelial disorders. Nature protocols. 2014; 9:2725–2731. [PubMed: 25356583]
25. Friedland AE, et al. Heritable genome editing in C. elegans via a CRISPR-Cas9 system. Nat Methods. 2013; 10:741–743. [PubMed: 23817069]
26. Starich TA, et al. Mutations affecting the chemosensory neurons of Caenorhabditis elegans. Genetics. 1995; 139:171–188. [PubMed: 7705621]
27. Williams CL, Masyukova SV, Yoder BK. Normal ciliogenesis requires synergy between the cystic kidney disease genes MKS-3 and NPHP-4. J Am Soc Nephrol. 2010; 21:782–793. [PubMed: 20150540]

28. Valente EM, et al. Mutations in TMEM216 perturb ciliogenesis and cause Joubert, Meckel and related syndromes. Nature genetics. 2010; 42:619–625. [PubMed: 20512146]
29. Kensche PR, van Noort V, Dutilh BE, Huynen MA. Practical and theoretical advances in predicting the function of a protein by its phylogenetic distribution. Journal of the Royal Society, Interface / the Royal Society. 2008; 5:151–170.
30. Iglesias A, et al. The usefulness of whole-exome sequencing in routine clinical practice. Genetics in medicine: official journal of the American College of Medical Genetics. 2014; 16:922–931. [PubMed: 24901346]
31. Shaheen R, et al. Identification of a Novel MKS Locus Defined By TMEM107 Mutation. Human molecular genetics. 2015
32. Nakada C, et al. Accumulation of anchored proteins forms membrane diffusion barriers during neuronal polarization. Nature cell biology. 2003; 5:626–632. [PubMed: 12819789]
33. Xu K, Zhong G, Zhuang X. Actin, spectrin, and associated proteins form a periodic cytoskeletal structure in axons. Science (New York N.Y. 2013; 339:452–456.
34. van Dam TJ, et al. Evolution of modular intraflagellar transport from a coatomer-like progenitor. Proceedings of the National Academy of Sciences of the United States of America. 2013; 110:6943–6948. [PubMed: 23569277]

Europe PMC Funders Author Manuscripts

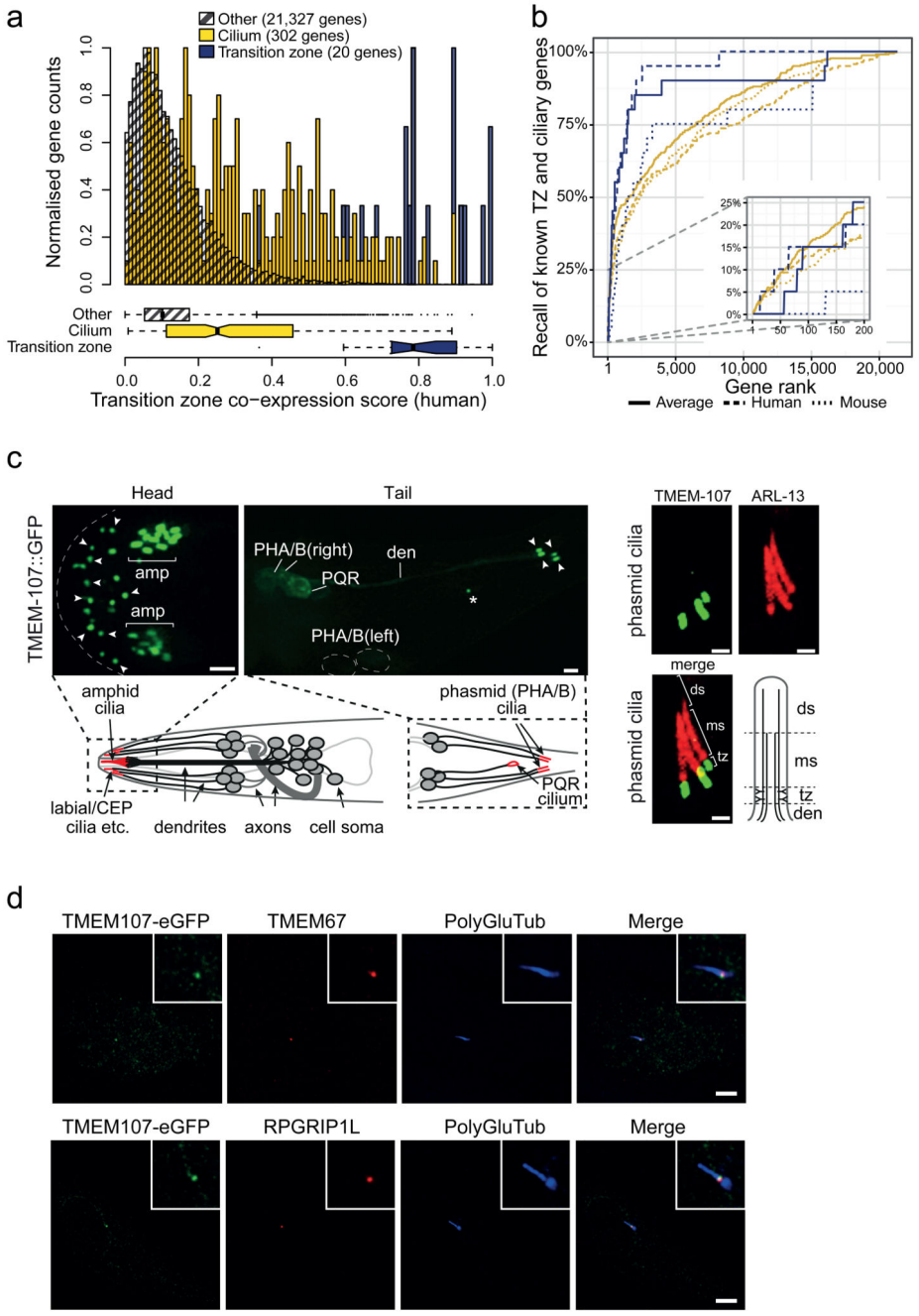

Figure 1. A weighted co-expression approach to discover TZ genes identifies TMEM107 as a TZ protein.

(a) Frequency histogram of binned human gene co-expression scores, derived from weighted analyses of gene expression datasets using a training set of 20 known TZ genes (Supplementary Table 1). Frequencies normalised to compare different distributions. SYSCILIA gold standard genes21 in yellow; TZ gene training in blue; all other genes in grey hatched. Box-plots display median and quartiles for histogram distributions. Whiskers (hashed lines) denote the minimum and maximum extent of the dataset. **(b)** Recall

Europe PMC Funders Author Manuscripts

performance (also known as sensitivity) of the co-expression approach retrieves known TZ (blue lines) and ciliary (yellow lines) genes. The graph shows that TZ genes can be retrieved compared to ciliary genes. Inset: recall performance for top 200 ranked genes. Ciliary genes taken from the SYSCILIA gold standard21. **(c)** *C. elegans* TMEM-107::GFP localises at the TZ. Shown are fluorescence images from worms expressing TMEM-107::GFP alone (left panels) or together with an ARL-13::tdTomato reporter (right panels). Left panels; accumulation of TMEM-107::GFP at the ciliary base region of 12 bilateral amphid cilia (amp; brackets), labial and CEP cilia (subset denoted by arrowheads), bilateral phasmid cilia (arrowheads) and the right-sided PQR cilium (asterisk) in the tail. Note that head schematic only shows a subset of the hermaphrodite's ciliated head neurons. Right panels; TMEM-107::GFP localises immediately proximal to middle segment (ms)-restricted ARL-13::tdTomato. Image shows all four phasmid cilia (left and right). Schematic denotes major subcompartments in phasmid cilia with microtubule doublets (only two shown) in the TZ and middle segments, and microtubule singlets in the distal segment (ds). den; dendrite. Bars; 2 μm (left two images), 1 μm (right images). **(d)** Human TMEM107 localises at the TZ. Shown are images of hTERT-RPE1 cells stably expressing GFP-tagged human TMEM107 (green) at a low level, costained with antibodies for ciliary axonemes (polyglutamylated tubulin; PolyGluTub) and the TZ (RPGRIP1L, TMEM67). Bars; 5 μm.

Europe PMC Funders Author Manuscripts

Europe PMC Funders Author Manuscripts

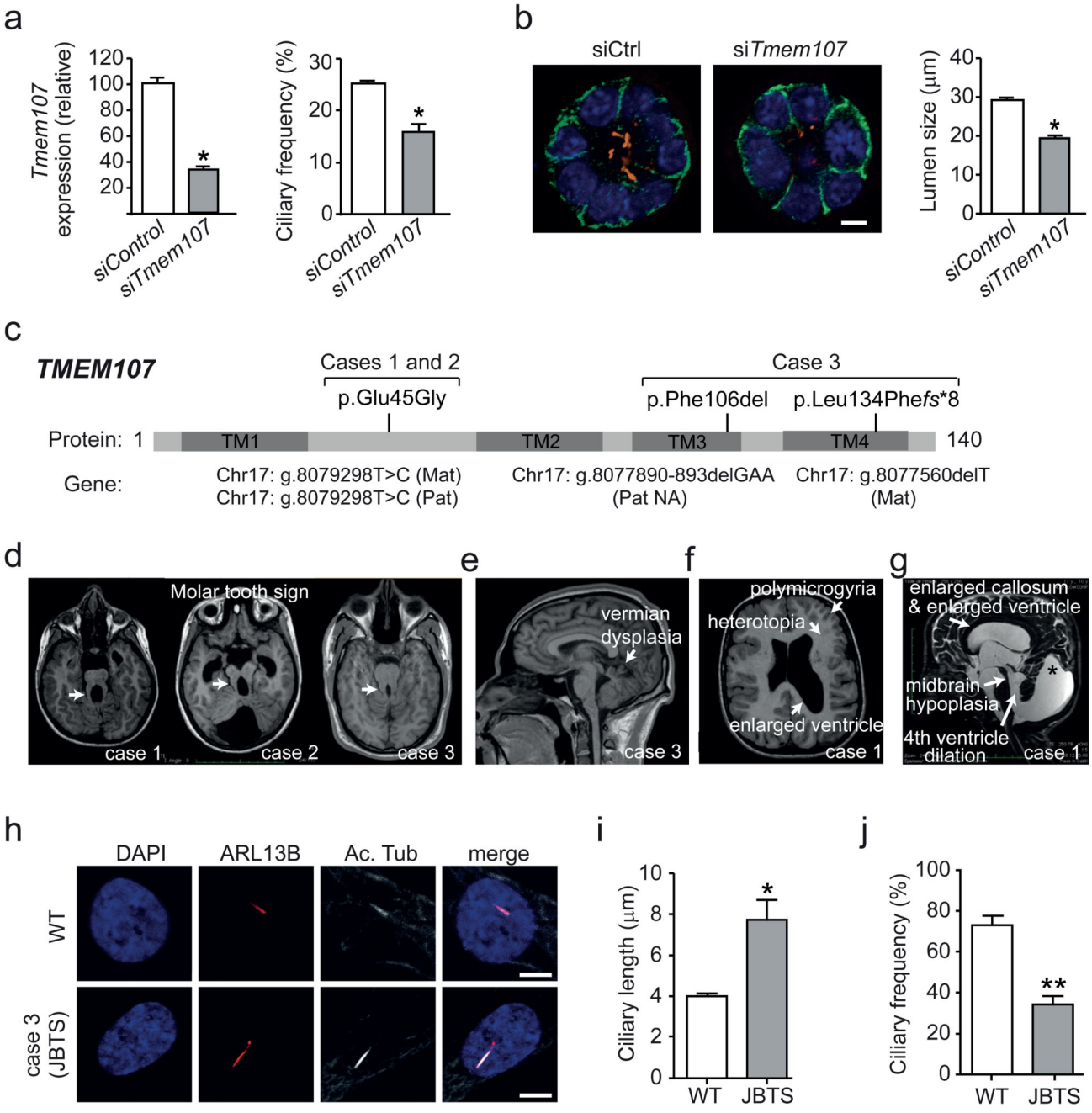

Figure 2. *TMEM107* regulates mammalian ciliogenesis and is mutated in OFDVI and JBTS individuals.

(a) IMCD3 cells transfected with *Tmem107* siRNA possess reduced *Tmem107* mRNA expression (vs scrambled siRNA control; qPCR data) and reduced mean ciliary frequency. Data represents mean ± S.E.M (n=350 cells, 1 experiment). *p<0.05 (unpaired t-test; vs control). **(b)** When grown in 3-D culture, IMCD3 cells transfected with *Tmem107* siRNA form spheroids with a reduced mean size. Cilia (orange) stained for acetylated alpha-tubulin; cell junctions (green) stained for beta-catenin. Data represents mean ± S.E.M (n=25

spheroids 2 independent experiments). *p<0.05 (unpaired t-test; vs control). Bar; 5 μm. **(c)** Schematic of human TMEM107 protein showing the position of identified patient mutations. Grey boxes correspond to the transmembrane domains. Mat; maternal, Pat; paternal, NA; not available. **(d)** Brain MRIs (axial views) showing the molar tooth sign, linked to elongated, thick and mal-oriented superior peduncles (white arrows) and hypoplastic vermis. **(e)** Brain MRI showing a dysplastic and highly hypoplastic vermis in sagittal view. A secondary enlargement of the fourth ventricle with displacement of the fastigium is also evident. **(f)** Brain MRI (axial view) showing heterotopias, enlarged lateral ventricles and polymicrogyria. (**g**) Brain MRI (sagittal view) showing enlarged posterior fossa (asterisk) with a cystic dilation of the fourth ventricle, a severe midbrain dysplasia and a thin corpus callosum with enlarged ventricles. **(h-j)** Shown in h are fibroblasts derived from skin biopsies of healthy control (wild type; WT) and patient 3 (JBTS) immunostained for cilia using antibodies against ARL13B (red; ciliary membrane) and acetylated tubulin (white; axonemal microtubules). Compared to control cells, JBTS cell cilia possess reduced lengths (i) and frequencies (j). Data represents mean ± S.E.M (n=10 (i) and 25 (j) cells pooled from 3 independent experiments).* p<0.05 (unpaired t-test; vs WT), ** p<0.01 (unpaired t-test; vs WT), bars; 5 μm.

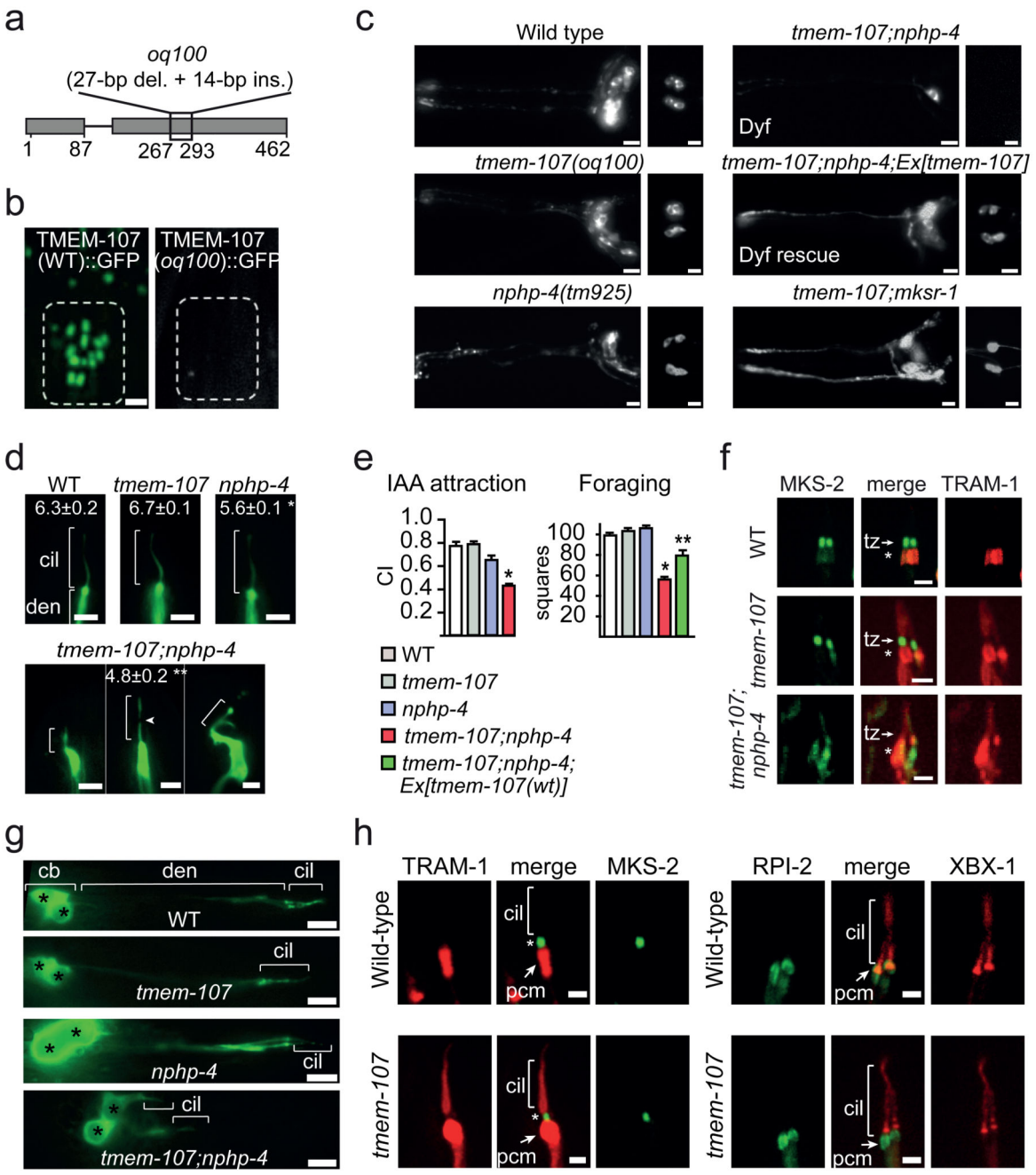

Figure 3. ***C. elegans tmem-107*** **controls diffusion barrier integrity and functions with** ***nphp-4*** **to regulate ciliary and TZ structural integrity.**

(a) Schematic of *oq100* Indel mutation in *tmem-107* gene. Exons denoted by grey boxes (numbers; nucleotide positions). del; deletion, ins; insertion. **(b)** *oq100* mutation disrupts TMEM-107 expression. Shown are amphid cilia TZs in worms expressing GFP-tagged wild-type or mutant (*oq100*) TMEM-107. Bar; 2 μm (images identically scaled). **(c)** Dye filling assay (measure of cilium integrity for 6 amphid (head) and 2 phasmid (tail) ciliated neurons) showing dye-filling defects (Dyf) in *tmem-107(oq100);nphp-4(tm925)* double mutants, but

Europe PMC Funders Author Manuscripts

not single mutants, or a *tmem-107(oq100);mkrs-1(tm3083)* double mutant. Dyf phenotype is rescued by expression of wild-type *tmem-107* (GFP-tagged; see Figure 1c). Bars; 10 μm. **(d)** Images of ASER neuronal cilia from worms expressing a *gcy-5p::gfp* that stains the ASER neuron. Numbers refer to cilium length measurements;mean ± S.E.M (n=28 (N2), 44 (*tmem-107*), 46 (*nphp-4*) and 81 (*tmem-107;nphp-4*) cilia). Brackets denote ciliary axonemes (cil). Arrowhead; occasional break in GFP staining observed only in double mutant. den; dendrite. * $p<0.01$ (unpaired t-test; vs WT), ** $p=0.01$ (unpaired t-test; vs *nphp-4*), Bars; 3 μm. **(e)** *tmem-107(oq100);nphp-4(tm925)* double mutants possess defects in cilia-related behaviours. Shown are population assays of isoamyl alcohol (IAA) attraction and single worm foraging assays. Data represents mean ± S.E.M. For IAA assays, n=30 (N2), 20 (*tmem-107*), 22 (*nphp-4*) and 29 (*tmem-107;nphp-4*); For foraging assays, n= 44 (N2), 43 (*tmem-107*), 63 (*nphp-4*), 54 (*tmem-107;nphp-4*) and 37 (*tmem-107;nphp-4;Ex[tmem-107(wt)]* * $p<0.01$ (unpaired t-test; vs WT), ** $p<0.01$ (unpaired t-test; vs *tmem-107;nphp-4*). CI; chemotaxis index. **(f)** TZ composition is altered in *tmem-107;nphp-4* double mutants. Shown are phasmid cilia from worms expressing TZ-localised MKS-2::GFP and periciliary membrane-localised, TRAM-1::tdTomato (asterisk). Bars; 2 μm. **(g)** *tmem-107(oq100);nphp-4(tm925)* double mutants possess short phasmid (PHA/B) dendrites and misplaced cilia. Neurons stained with OSM-6(IFT52)::GFP. Cil; ciliary axonemes, den; dendrite, cb; cell bodies (also denoted by asterisks). Brackets denote PHA/B cilia. Bars; 5 μm. **(h)** TZ membrane diffusion barrier is selectively disrupted in *tmem-107(oq100)* mutants. Shown are phasmid cilia from worms expressing TRAM-1::tdTomato (and MKS-2::GFP; marks TZ) (left images) or RPI-2::GFP (and XBX-1::tdTomato; marks cilia) (right images). TRAM-1 (translocon subunit) and RPI-2 (retinitis pigmentosa 2) are excluded from wild-type (WT) cilia, whereas TRAM-1 (but not RPI-2) leaks into *tmem-107(oq100)* cilia. Asterisk; TZ localization of MKS-2, pcm; periciliary membrane, cil; ciliary axoneme. Bars; 2 μm.

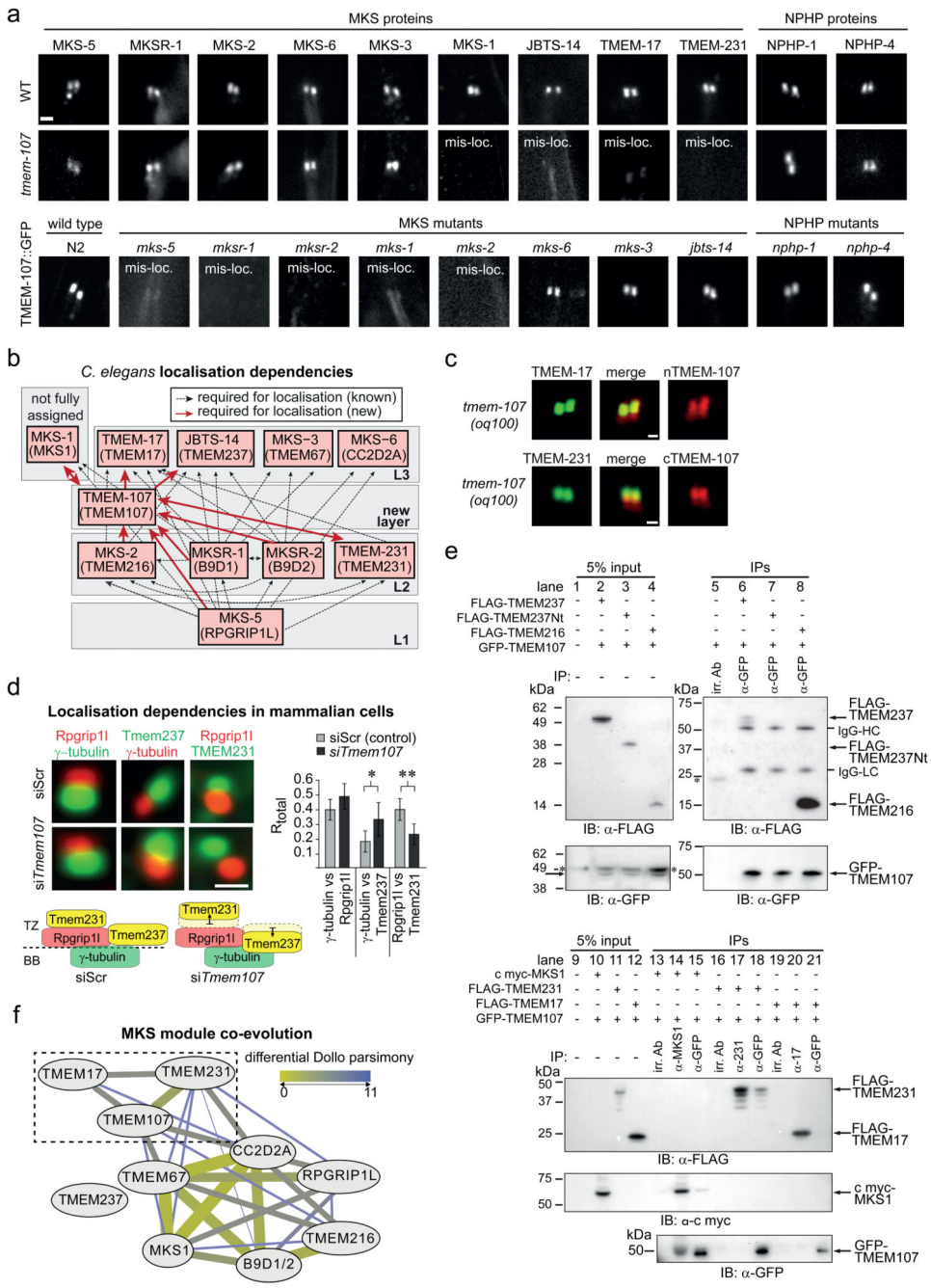

Figure 4. Evolutionary conserved association of TMEM107 with the TZ-localised MKS module.

(a) Phasmid TZ localisations of GFP-tagged MKS and NPHP module proteins in WT and *tmem-107(oq100)* mutant worms, and TMEM-107::GFP in MKS and NPHP mutants. Bar; 1 μm (all images similarly scaled). mis-loc.; mislocalised. **(b)** Schematic summarising TZ localisation dependencies in (a). TMEM-107 positioned at an intermediate level within a hierarchical three layer (L1-3) MKS module assembly model (drawn based on refs10, 13, 15, 19; MKS-1 'unassigned' because hierarchical analysis has not yet been conducted using an *mks-1* null allele). Human orthologues denoted in brackets. **(c)** Expression of

Europe PMC Funders Author Manuscripts

TMEM-107::RFP with disrupted cytosolic N- or C- termini (nTMEM-107, cTMEM-107; see methods) rescues mislocalised TMEM-17::GFP and TMEM-231::GFP in *tmem-107(oq100)* mutants. Shown are phasmid cilia TZs. Bar; 0.5 μm. **(d)** *Tmem107* depletion (siRNA) in IMCD3 cells disrupts relative localisations of endogenous MKS module proteins. Cells double-stained as indicated and colocalisation determined as an R_{total} Pearson correlation value (FIJI "Colocalization Threshold" plugin). In *Tmem107* depleted cells, Rpgrip1l localisation is unaffected (relative to basal body (BB) γ-tubulin), whereas Tmem231and Tmem237 proteins shift (black arrows) relative to γ-tubulin or Rpgrip1l. Data in graph represents mean ± S.E.M (n=150 cells pooled from 3 independent experiments). siScr; siRNA scrambled control. ** $p<0.01$, * $p<0.05$ (unpaired t-test; vs siScr control). Bar; 1 μm. **(e)** Coimmunoprecipitation (coIP) assays in IMCD3 cells. Upper panels, lanes 1-4: input material from whole cell extracts (WCEs) transfected with the indicated constructs and immunoblotted (IB) with anti-GFP or anti-FLAG. Lanes 5-8: proteins immunoprecipitated (IP) by an irrelevant antibody (irr. Ab; anti-MICU3) or anti-GFP, and then immunoblotted for FLAG or GFP. IgG heavy chain (HC) and light chain (LC) in coIPs are indicated. Asterisks (*) mark non-specific proteins. Lower panels, lanes 9-12: input WCE showing expression of FLAG-TMEM231, FLAG-TMEM17 and c myc-MKS1. Lanes 13-21: IPs with antibodies against MKS1 (lane 14), TMEM231 (231; lane 17) and TMEM17 (17; lane 20) and then immunoblotted as indicated. Note that although TMEM107 co-IP's TMEM231, TMEM231 does not co-IP detectable levels of TMEM107. **(f)** Co-evolution relationships between MKS components using differential Dollo parsimony that counts along a phylogenetic tree how often two genes are lost independently from each other. Thickness and color gradient indicate strong co-evolution. Edges with differential Dollo parsimony scores >11 are not shown. Dashed box: co-evolving MKS submodule.

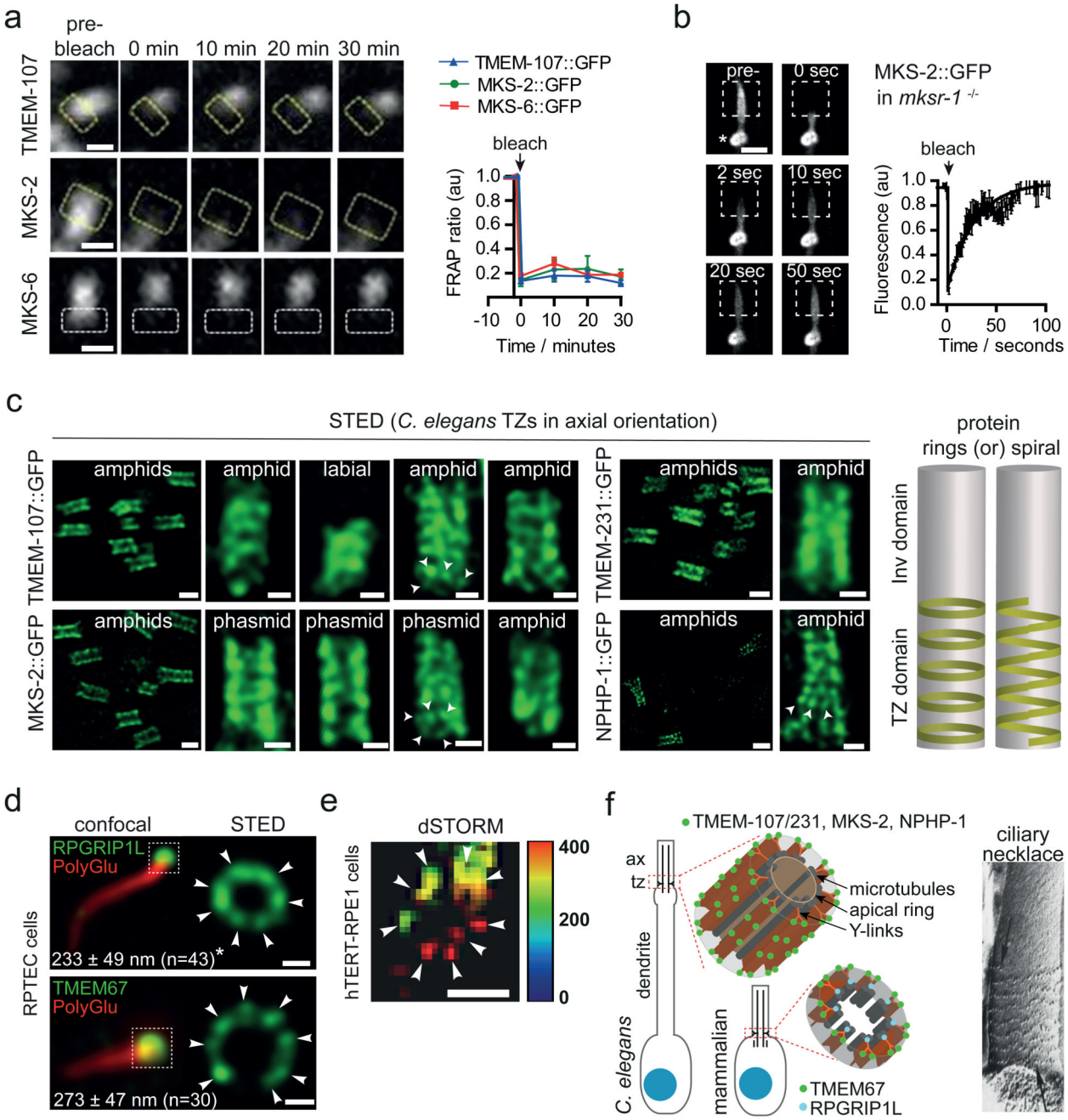

Figure 5. Anchoring and periodic distributions of MKS module proteins within the TZ.

(a) GFP-tagged TMEM-107, MKS-2 and MKS-6 are immobile within the *C. elegans* TZ. Shown are fluorescence recovery after photobleaching (FRAP) curves and representative time-lapse images after photobleaching one half of a TZ signal (boxed region). Data points represented as mean ± S.E.M. (n=3 (MKS-6) or 4 (TMEM-107, MKS-2) independent experiments). Bar; 500 nm. **(b)** *C. elegans* MKS-2 immobility depends on MKS module proteins. Shown is a FRAP curve and representative time-lapse images (phasmid cilia) after photobleaching MKS-2::GFP signals (boxed region) in an *mksr-1* mutant. Asterisk;

periciliary membrane. Data points represented as mean ± S.E.M. (n=4 independent experiments). au; arbitrary units, Bar; 2 μm. **(c)** Arrowheads; independent signal clusters within a ring-like domain. Bars; 200 nm (high magnification images), 500 nm (low magnification images). **(d)** STED images of endogenous human RPGRIP1L and TMEM67 in renal RPTEC cells showing clusters (arrowheads) of protein in a single ring of differing diameters (mean ± S.D.) at the TZ. Corresponding confocal images co-stained for cilia with polyglutamylated tubulin antibody. *p=0.001 (unpaired t-test; vs TMEM67). Bars; 100 nm. **(e)** dSTORM of human RPGRIP1L (visualised with AlexaFluor647) with 10 nm binning, image smoothing and contrast enhancement in FIJI (raw images shown in Supplementary Figure 5d), showing periodic localisation (arrowheads) in a loose ring at the TZ. Image depth-coded by colour. Z-axis scale bar (nm) on right. Bar; 100 nm. **(f)** Models. MKS module proteins (and *C. elegans* NPHP-1) occupy periodic radial and axial TZ subdomains. Mammalian RPGRIP1L and TMEM67 localise as independent clusters, forming a single ring domain at the TZ core (RPGRIP1L) or membrane (TMEM67). *C. elegans* MKS and NPHP proteins also localise as discrete independent clusters, forming multiple ring domains (or possible spiral domains) along the TZ length. The nematode axial distribution may correspond to the ciliary necklace (TEM example from ref12). Periodicity and immobility of MKS module proteins suggests association with Y-links, which form extended sheets in *C. elegans* (Supplementary Video 1) and are implicated in necklace formation.